Journal of Controlled Release 244 (2016) 229–239

Contents lists available at ScienceDirect

Journal of Controlled Release

journal homepage: www.elsevier.com/locate/jconrel

# Bioresponsive and fluorescent hyaluronic acid-iodixanol nanogels for targeted X-ray computed tomography imaging and chemotherapy of breast tumors

Yaqin Zhu [a,b], Xiuxiu Wang [a], Jing Chen [a], Jian Zhang [a], Fenghua Meng [a], Chao Deng [a], Ru Cheng [a], Jan Feijen [a,b,*], Zhiyuan Zhong [a,*]

[a] Biomedical Polymers Laboratory, and Jiangsu Key Laboratory of Advanced FunctionalPolymer Design and Application, College of Chemistry, Chemical Engineering and MaterialsScience, Soochow University, Suzhou, 215123, PR China

[b] Department of Polymer Chemistry and Biomaterials, Faculty of Science and Technology, MIRA Institute for Biomedical Technology and Technical Medicine, University of Twente, P.O. Box 217, 7500, AE, Enschede, The Netherlands

ARTICLE INFO

*Article history:*
Received 13 June 2016
Received in revised form 18 August 2016
Accepted 22 August 2016
Available online 25 August 2016

*Keywords:*
Nanogels
Hyaluronic acid
X-ray computed tomography
Reduction-sensitive
Cancer
Paclitaxel

ABSTRACT

Nanotheranostics is a rapidly growing field combining disease diagnosis and therapy, which ultimately may add in the development of 'personalized medicine'. Here, we designed and developed bioresponsive and fluorescent hyaluronic acid-iodixanol nanogels (HAI-NGs) for targeted X-ray computed tomography (CT) imaging and chemotherapy of MCF-7 human breast tumors. HAI-NGs were obtained with a small size of ca. 90 nm, bright green fluoresence and high serum stability from hyaluronic acid-cystamine-tetrazole and reductively degradable polyiodixanol-methacrylate via nanoprecipitation and a photo-click crosslinking reaction. Notably, paclitaxel (PTX)-loaded HAI-NGs showed a fast glutathione-responsive drug release. Confocal microscopy displayed efficient uptake of HAI-NGs by CD44 overexpressing MCF-7 cells via a receptor-mediated mechanism. MTT assays revealed that HAI-NGs were nontoxic to MCF-7 cells even at a high concentration of 1 mg/mL whereas PTX-loaded HAI-NGs exhibited strong inhibition of MCF-7 cells. The *in vivo* pharmcokinetics, near-infrared imaging and biodistribution studies revealed that HAI-NGs significantly prolonged the blood circulation time and enhanced tumor accumulation of PTX. Interestingly, significantly enhanced CT imaging was observed for MCF-7 breast tumors in nude mice via either intratumoral or intravenous injection of HAI-NGs as compared to iodixanol. HAI-NGs fluoresence was distributed thoughout the whole tumor indicating deep tumor penetration. PTX-loaded HAI-NGs showed effective suppression of tumor growth with little systemic toxicity. HAI-NGs appear as a "smart" theranostic nanoplatform for the treatment of CD44 positive tumors.



## 1. Introduction

Theranostic nanomedicines contain both a diagnostic agent and one or more therapeutic drugs within one integrated system, enabling non-invasive diagnosis, therapy, and real-time monitoring of the therapeutic response at the same time [1–4]. Among various imaging techniques, computed tomography (CT) is one of the most commonly used non-invasive clinical imaging modalities because of its wide availability, high spatial resolution, unlimited depth, and accurate anatomical information with reconstructed three dimensional imaging [5–7]. Iodixanol (Visipaque) is a small iodinated molecule, clinically used as a CT contrast agent that has a low osmolality and great tolerability [8]. However, like all low molecular weight iodinated CT contrast agents, iodixanol has drawbacks like non-specific distribution and rapid renal clearance following *i.v.* injection [9]. In recent years, nanosized CT contrast agents have attracted great interest as they have several advantages over small molecular contrast agents such as prolonged circulation time, site-specific accumulation and use for theranostics [10–13]. Some recent work showed systems with great promise of nanosized CT contrast agents such as iodinated hyaluronic acid oligomer-based nano-assembled systems, theranostic self-assembly structures of gold nanoparticles, and multifunctional dendrimer-entrapped gold nanoparticles for simultaneous tumor imaging and therapy [14–16].

Among various types of nanoscale drug delivery systems, nanogels have attracted increasing attention since they have a large surface area for multivalent bioconjugation and a crosslinked three-dimensional network structure that offers great colloidal stability [17–19]. To

* Corresponding authors at: Biomedical Polymers Laboratory, College of Chemistry, Chemical Engineering and Materials Science, Soochow University, Suzhou, 215123, PR China.

*E-mail addresses:* j.feijen@tnw.utwente.nl (J. Feijen), zyzhong@suda.edu.cn (Z. Zhong).

http://dx.doi.org/10.1016/j.jconrel.2016.08.027
0168-3659/

achieve rapid release of the payload at the target site, pH, redox potential, and enzyme-responsive nanogels have been designed [20–27]. Nanogels based on hyaluronic acid (HA) have recently appeared as a unique system because HA is a hydrophilic natural material with excellent biocompatibility and intrinsic targeting ability toward CD44-overexpressing tumor cells [26,28–31]. HA nanoparticles have been used for efficient delivery of chemotherapeutics, proteins as well as siRNA *in vitro* and *in vivo* [32–35].

In this paper, we report on bioresponsive and fluorescent hyaluronic acid-iodixanol nanogels (HAI-NGs) for targeted CT imaging and chemotherapy of MCF-7 human breast tumor (Scheme 1). HAI-NGs were obtained from hyaluronic acid-cystamine-tetrazole (HA-Cys-Tet) and reductively degradable polyiodixanol-methacrylate (SS-PI-MA) *via* nanoprecipitation and a photo-click crosslinking reaction. HAI-NGs were designed with the following unique features: i) both HA and iodixanol have excellent biocompatibility and are currently used in the clinic; ii) the "tetrazole-ene" photo-click crosslinking reaction is highly selective, which prevents cross-reaction with most drugs and furthermore endows nanogels with bright green fluorescence [36,37]; iii) HA can actively target CD44 receptors which are overexpressed on various malignant tumor cells and stem cells [38–41]; iv) HAI-NGs can be used for targeted CT imaging *in vivo*; and v) the reduction-sensitivity of HAI-NGs allows fast intracellular release of payloads like PTX to achieve efficient and targeted chemotherapy. Herein, the stability of HAI-NGs and the reduction-triggered PTX release from PTX loaded HAI-NGs were investigated. Furthermore, the targetability of HAI-NGs and antitumor activity of PTX loaded HAI-NGs toward MCF-7 cells, the pharmacokinetics and biodistribution, NIR and CT imaging, as well as therapeutic effects in MCF-7 human breast tumor xenografts in mice were evaluated.

## 2. Materials and methods

### 2.1. Materials

Sodium salt of hyaluronic acid (HA, molecular weight: 35 kDa, Shandong Freda Biopharm Co., Ltd., Shangdong, China), 1-(3-dimethylaminopropyl)-3- ethylcarbodiimide hydrochloride (EDC·HCl, 98%, J&K, Beijing, China), N-hydroxysuccinimide (NHS, 98%, Alfa Aesar, USA), cystamine dihydrochloride (Cystamine·2HCl, >98%, Alfa Aesar, USA), *N*, *N*-dimethylformamide (DMF, anhydrous, >99.7%, Alfa Aesar), paclitaxel (PTX, >99%, Beijing ZhongShuo Pharmaceutical Technology Development Co., Ltd., Beijing, China), iodixanol (99.3%, Hubei Ju Sheng Technology Co., Ltd., Hubei, China), methacrylic anhydride (MA, 94%, J&K, Beijing, China), 4-dimethylamino pyridine (DMAP, 99%, Alfa Aesar, USA), dibutyltin dilaurate (DBTDL, 97.5%, J&K, Beijing, China), acetonitrile (99.3%, HPLC grade, Merck, Germany), glutathione (GSH, >98%, Amresco, USA), dithiothreitol (DTT, 99%, Merck, Germany), cyanine 5 (Cy5, 98%, Lumiprobe, USA), goat serum (Roche, Germany), 3-(4,5-dimethylthiazol-2-yl)-2,5-diphenyltetrazolium bromide (MTT, Sigma, USA), DAPI (Invitrogen, USA), trypsin (Jinuo Biomedical Technology, Hangzhou, Zhejiang, China), rat monoclonal *anti*-mouse CD31 (BD Pharmingen, San Jose, California, USA), Alexa 594 conjugated donkey anti-rat secondary antibody (Molecular Probes, Eugene, OR, USA), cell culture dishes and 24 and 96-well plates (Thermo Fisher Scientific, USA) were used as received. Pyridine, diethyl ether, dichloromethane (DCM), dimethyl sulfoxide (DMSO), *N*, *N*-Dimethyl formamide (DMF), and methanol were obtained from Sinopharm Chemical Reagent Co., Ltd., Shanghai, China. Tetrazole (Tet) and cystamine diisocyanate (CDI) were synthesized according to our previous reports [36,42].

### 2.2. Cell culture and animal studies

MCF-7 breast cancer cells and L929 murine fibroblastic cells were purchased from the cell bank of the Chinese Academy of Sciences (Shanghai, China). Cells were maintained in DMEM medium (HyClone, Logan, Utah, USA) supplemented with 1% penicillin, 1% streptomycin (Jinuo Biomedical Technology, Hangzhou, Zhejiang, China), and 10% fetal bovine serum (FBS, Gibco, Invitrogen, USA). The cells were cultured as a monolayer in a humidified atmosphere containing 5% $CO_2$ at 37 °C.

Female Balb/c nude mice of 4-6 weeks age were purchased from Model Animal Research Center of Nanjing University. Mice were housed at 25 °C and 55% humidity under natural light/dark conditions and allowed free access to standard food and water. All animal procedures were performed following the protocol approved by the Animal Study Committee of Soochow University.

### 2.3. Synthesis of reductively degradable polyiodixanol-methacrylate (SS-PI-MA)

SS-PI-MA was readily synthesized *via* polyaddition of iodixanol and cystamine diisocyanate (CDI) followed by treatment with methacrylic anhydride (MA). Briefly, in a glove-box under a nitrogen atmosphere, iodixanol (500 mg, 0.32 mmol) was dissolved in anhydrous DMF

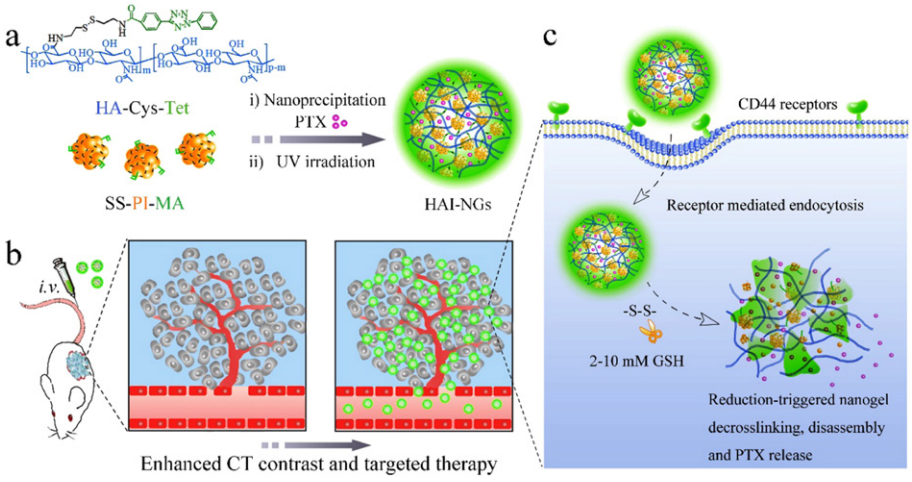


**Scheme 1.** Illustration of bioresponsive and fluorescent hyaluronic acid-iodixanol nanogels for targeted X-ray computed tomography imaging and chemotherapy of breast tumors. (a) PTX-loaded HAI-NGs are prepared *via* nanoprecipitation followed by crosslinking *via* UV irradiation; (b) PTX-loaded HAI-NGs actively target and accumulate at MCF-7 tumors, resulting in enhanced CT contrast and targeted therapy; (c) PTX-loaded HAI-NGs are selectively internalized into the MCF-7 breast tumor cells *via* CD44 receptor-mediated endocytosis, nanogels are decrosslinked and disassembled in response to GSH in the cytosol, and PTX is quickly released into the cells.

(15 mL) in a 50-mL round-bottomed flask. CDI (130.6 mg, 0.64 mmol) and dibutyltin dilaurate (DBTDL, 31.5 mg, 0.05 mmol) were added. The mixture was stirred at 65 °C for 24 h. The resulting polymer was isolated by precipitation from cold diethyl ether, filtration and dried *in vacuo* at r.t. To completely remove unreacted iodixanol, SS-PI polymer was dissolved in DMF (5 mL) and precipitated in cold methanol, filtrated and dried *in vacuo* at r.t. Yield: 85.4%. $^1$H NMR (DMSO-$d_6$): iodixanol moieties: $\delta$ 1.76, 3.89-4.0, 4.75, 5.10, 7.27, 8.81; CDI moieties: $\delta$ 2.83, 3.27.

SS-PI (200 mg) was dissolved in DMF (5 mL) in a nitrogen environment. Methacrylic anhydride (5 μL) and DMAP (5 mg) were added. The mixture was stirred at 30 °C for 36 h. The resulting polymer was isolated by precipitation from cold DCM, filtration and dried *in vacuo* at r.t. Yield: 87.5%. $^1$H NMR (DMSO-$d_6$): iodixanol moieties: $\delta$ 1.76, 3.89–4.0, 4.75, 5.10, 7.27, 8.81; CDI moieties: $\delta$ 2.83, 3.27; MA moieties: $\delta$ 1.89, 5.70, 6.07.

### 2.4. Synthesis of HA-Cys-Tet

Tet-Cys-$NH_2$ was obtained by selective coupling of Tet to one of the primary amino groups of cystamine. Firstly, cystamine dihydrochloride (1.2 g, 5.3 mmol) dissolved in DMF (10 mL) was desalted by adding excess $Et_3N$ (2 mL) and stirred at r.t. for 30 min. The carboxyl group of Tet (0.27 g, 1 mmol) was activated for 15 min by EDC and NHS in DMF (10 mL). Activated Tet was added dropwise into the stirred cystamine solution in DMF. The mixture was stirred at 30 °C for 24 h and filtrated to remove $Et_3N\cdot HCl$. The red supernatant was precipitated in deionized water. The precipitates were collected by centrifugation and washed three times with deionized water to remove excess cystamine and finally lyophilized. Yield: 92.1%. $^1$H NMR (400 MHz, $CDCl_3$, $\delta$): 8.87 (t, —CON*H*—), 8.25, 8.16 (dd, dd, —$C_6H_4$—CONH—), 8.06, 7.71, 7.64 (dd, t, t, $C_6H_5$—$N_4C$—), 3.59 (dd, —CONH—$CH_2$—), 2.96 (t, —$CH_2$—S—), 2.78 (t, —$CH_2$—$NH_2$).

HA-Cys-Tet was synthesized by conjugating Tet-Cys-$NH_2$ to HA *via* amidation. Firstly, HA (100 mg, 2.9 nmol) was dissolved in deionized water (5 mL) and then EDC (153.5 mg, 0.8 mmol) and NHS (46 mg, 0.4 mmol) were added to activate the carboxyl groups of HA. After 30 min, DMSO (10 mL) was added. Tet-Cys-$NH_2$ (70 mg, 0.175 mmol) dissolved in DMSO (5 mL) was added dropwise into the stirred $H_2O$/DMSO mixture. The reaction mixture was kept at 35 °C for 48 h. Subsequently, the reaction mixture was dialyzed against DMSO for 48 h to remove unreacted Tet-Cys-$NH_2$, dialyzed against deionized water for 48 h and finally lyophilized. Yield: 90.3%. $^1$H NMR (DMSO-$d_6$: $D_2O$ = 1:1): HA moieties: $\delta$ 1.81, 3.01-3.65; cystamine moieties: $\delta$ 2.27, 2.71; Tet moieties: $\delta$ 7.61–8.22.

### 2.5. Characterization

$^1$H NMR spectra were recorded on a Unity Inova 400 spectrometer (Agilent, USA) operating at 400 MHz using deuterium oxide ($D_2O$, CIL, Andover, MA, USA) or deuterated dimethylsulfoxide (DMSO-$d_6$, CIL, Andover, MA, USA) as a solvent. The molecular weight and polydispersity of the copolymers were determined using a gel permeation chromatograph (GPC) instrument (Waters 1515, USA) equipped with two linear PL gel columns (500 Å and Mixed-C) following a guard column and a differential refractive-index detector (RI 2414). The measurements were performed using DMF as the eluent at a flow rate of 1.0 mL/min at 30 °C and a series of narrow poly (methyl methacrylate), (PMMA) standards for the calibration of the columns. The size of nanogels was determined using dynamic light scattering (DLS). Measurements were carried out at 25 °C using a Zetasizer Nano-ZS from Malvern Instruments equipped with a 633 nm He—Ne laser using back-scattering detection. Transmission electron microscopy (TEM) was performed using a Tecnai G220 TEM operated at an accelerating voltage of 200 kV. PTX concentrations were determined by HPLC (Shimadzu LC20AD, Japan) with UV detection at 227 nm using a mixture of acetonitrile and water (v/v = 1/1) as the mobile phase.

### 2.6. Preparation and characterization of nanogels

HA-Cys-Tet (10 mg/mL in DMSO) and SS-PI-MA (10 mg/mL in DMSO) at a weight ratio of 1:4 were injected directly into magnetically stirred PB (5 mL, 10 mM, pH 7.4) buffer. The obtained bluish dispersions were transferred to a plastic round disk and exposed to UV light (Intelliray 400, Shenzhen Wisbay M&E Co., Ltd., Shenzhen, China) at 50 mW/cm$^2$ for 60 s. The resulting nanogels (HAI-NGs) were dialyzed against PB buffer for 12 h. The size of HAI-NGs was determined by DLS.

PTX-loaded HAI-NGs and Cy5-loaded HAI-NGs were also prepared as described above except that PTX solution (10 mg/mL in DMSO) or Cy5 solution (5 mg/mL in DMSO) was added to the solution of the polymer (10 mg/mL in DMSO) at a theoretical drug loading content (DLC) of 10 wt.%. To determine the DLC and drug loading efficiency (DLE), 50 μL of PTX-loaded nanogel was treated with DTT solution in water (50 μL, 20 mM). Acetonitrile (450 μL) was added and the mixture was centrifuged at 12,000 rpm for 10 min., The PTX concentration in the supernatant was determined by HPLC. DLC and DLE were determined according to the following formulas:

$$\text{DLC (wt.\%)} = (\text{weight of loaded drug/total weight of polymer and loaded drug}) \times 100$$

$$\text{DLE (\%)} = \text{weight of loaded drug/weight of drug in feed} \times 100$$

### 2.7. Reduction-triggered drug release

The *in vitro* release of PTX from HAI-NGs was studied using a dialysis tube (Spectra/Pore, MWCO 12,000) at 37 °C in PB (10 mM, pH 7.4) either in the presence or absence of 10 mM GSH. To acquire sink conditions, drug release studies were performed with HAI-NGs dispersions (0.5 mL) with an initial PTX concentration of 50 μg/mL, which were dialyzed against 25 mL of the media mentioned above. At desired time intervals, 5 mL of release medium was taken out and replenished with an equal volume of fresh medium. The amount of PTX released was determined by HPLC. The *in vitro* release of Cy5 from HAI-NGs was studied using a dialysis tube (Spectra/Pore, MWCO 12,000) at 37 °C in PB (10 mM, pH 7.4) in the presence of 10% FBS. The amount of Cy5 released was determined by fluorescence spectroscopy (Cary Eclipse, Agilent Technologies).

### 2.8. MTT assay

The antitumor activity of PTX-loaded HAI-NGs and free PTX was determined by MTT assays. Briefly, MCF-7 cells were seeded at a density of $5 \times 10^3$ cells/well in 96-well plates for 24 h. The prescribed amounts of PTX-loaded HAI-NGs or free PTX in ethanol and Cremophor EL (1/1, v/v) was added. The cells were incubated for 4 h, the medium was removed and replaced with fresh medium, and cells were incubated for another 44 h. Competition studies were performed by pre-treating cells with free HA polymer (5 mg/mL) for 4 h prior to incubation with PTX-loaded HAI-NGs. Subsequently, MTT stock solution (20 μL, 5 mg/mL) was added to each well, and the plates were further incubated for 4 h at 37 °C in the dark. The medium was discarded and DMSO (150 μL) was added to dissolve the blue formazan crystals. Cell viability was assessed by the absorbance at 492 nm of the DMSO solution measured on a microplate reader. The data were expressed as the percentages of viable cells compared to the survival of a control group (untreated cells).

### 2.9. Cellular uptake study

Cellular uptake of HAI-NGs was analyzed by confocal laser scanning microscopy (CLSM, Leica TCS SP5, Wetzlar, Germany). Briefly, MCF-7 cells or L929 cells were seeded on round glass coverslips at a density of $5 \times 10^4$ cells/well in 24-well plates and cultured at 37 °C for 24 h. HAI-NGs (final concentration: 1 mg/mL) were added and incubated with the cells for 1, 2 or 4 h. Competition experiments were performed by pre-treating cells with free HA polymer (5 mg/mL) for 4 h prior to incubation with HAI-NGs. The culture medium was removed and the cells were washed three times with PBS. Then cells were fixed using 4% paraformaldehyde, treated with DAPI for 10 min for nuclei staining and finally examined with CLSM.

### 2.10. In vivo pharmacokinetics

The mice were handled using protocols approved by Soochow University Laboratory Animal Center and the Animal Care and Use Committee of Soochow University. The PTX level in blood was measured by withdrawing ~20 μL of blood from the tail vein of nude mice at different time points post injection of PTX-loaded HAI-NGs or free PTX (5 mg PTX equiv./kg). Each blood sample was dissolved in lysis buffer (0.15 mL, 1% Triton X-100) with brief sonication. PTX was extracted by incubating blood samples in methanol (0.6 mL) at −20 °C overnight. The samples were vortexed and centrifuged at 18,000 rpm for 15 min. The PTX level of the supernatant was determined by HPLC.

### 2.11. In vivo near-infrared fluorescence imaging

Tumor-bearing mice were established by subcutaneously injecting about $1 \times 10^7$ MCF-7 cells into the back of the mice. Tumors were allowed to grow to an average size of about 100 $mm^3$ in diameter before the experiments. To investigate the tumor targeting efficacy of HAI-NGs *in vivo*, Cy5-loaded HAI-NGs (200 μL, Cy5 concentration: 25 μg/mL) were injected into the tumor-bearing mice *via* the tail vein. At 2, 4, 6, 12 and 24 h post injection, the mice were anesthetized with 1% pentobarbital sodium, and whole body fluorescence images were acquired using a near-infrared fluorescence imaging system (Caliper IVIS Lumina II, Ex 633 nm, Em 670 nm).

### 2.12. Biodistribution

To quantify the amount of PTX delivered to the tumor and different organs, MCF-7 tumor-bearing mice following 6 or 12 h *i.v.* injection with PTX-loaded HAI-NGs or free PTX (5 mg PTX equiv./kg) were sacrificed. The tumor and organs including heart, liver, spleen, lung, and kidney were collected, washed with cold saline, weighed, and then homogenized in 1 mL of methanol. PTX was extracted by incubating with methanol at −20 °C overnight. After vortexing and centrifugation at 12,000 rpm for 15 min, the PTX level in the supernatant was determined by HPLC.

### 2.13. CT imaging

MCF-7 breast tumor bearing mice were used for CT imaging. The CT imaging was performed with a GE discovery CT750 HD (GE Healthcare, WI) with beam collimation of 64 × 0.625 mm, table speed of 27 mm per rotation, beam pitch of 1.25 and gantry rotation time of 1.0 s. The mice were anesthetized with 1% pentobarbital sodium, placed prone on the imaging bed and underwent CT imaging. HAI-NGs or iodixanol solution was intravenously injected into the mice at a dose of 60 mg iodine equiv./kg. Whole-body images were obtained at 0, 7, 9, and 11 h post injection.

### 2.14. Immunofluorescent analysis for tumor penetration

Nude mice bearing MCF-7 breast cancer xenografts were used to investigate the tumor penetration behavior of the nanogels. When the tumor size reached a size of about 150 $mm^3$, intrinsic fluorescent HAI-NGs (200 μL, 10 mg/mL) were injected into the tumor-bearing mice *via* the tail vein. At various time points (2, 6 and 12 h) post injection, MCF-7 tumors were harvested, fixed in 4% formalin overnight, embedded in paraffin, and sliced for immunofluorescent staining analysis. In brief, paraffin of the tissue slices was removed by xylene for 15 min twice followed by successive rehydration in ethanol, 90% ethanol, 70% ethanol and deionized water for 5 min twice, respectively. Then, the slices were incubated in 10 mM citrate buffer solution at 100 °C for 10 min. After cooling down to room temperature and washing with PBS, the slices were incubated with 10% goat serum solution in the dark at 4 °C overnight and then exposed to the appropriate primary monoclonal antibody (1:100 dilution in PBS) for 1 h in a humidified chamber at 37 °C followed by washing three times with PBS. The slices were then counterstained with an Alexa 594 conjugated donkey anti-rat secondary antibody (1:500 dilution in PBS) in a humidified chamber at 37 °C for 1 h, followed by washing three times with PBS and staining with DAPI (5 μg/mL) for 10 min. Finally, the stained slices were observed under a CLSM imaging system (Leica TCS SP5, Wetzlar, Germany) using a 60 × oil immersion objective.

### 2.15. In vivo antitumor efficacy

Nude mice bearing MCF-7 breast cancer xenografts were used to evaluate the therapeutic efficacy of PTX-loaded HAI-NGs. The treatments were initiated when the tumor reached a volume of 30–40 $mm^3$. The day starting the treatment was designated as day 0. On day 0, the mice were randomly divided into three groups of 6 mice and injected intravenously *via* the tail vein with PTX-loaded HAI-NGs (5 mg PTX equiv./kg). The treatment was repeated every 3 days for a total of 5 doses. The tumor sizes were measured by calipers and the volume was calculated according to the formula $V = 0.5 \times L \times W \times H$, wherein L, W and H are the tumor dimensions at the longest, widest and highest direction, respectively. Mice were weighed and the relative body weights were normalized to their initial weights. Mice in each group were considered to be dead either when the tumor volume increased to 1000 $mm^3$, or when the mice died during treatment. At the end of the treatment, one mouse of each group was sacrificed, and the tumor, liver, heart and kidney were excised. The tissues were fixed with 4% formalin solution and embedded in paraffin. The sliced organ tissues (thickness: 4 mm) mounted on glass slides were stained by hematoxylin and eosin (H&E) and observed with a digital microscope (Leica QWin, Germany).

### 2.16. Statistical analysis

All data are presented as the mean ± standard deviation (SD). One-way analysis of variance (ANOVA) was used to determine significance among groups, after which post-hoc tests with the Bonferroni correction were used for comparison between individual groups. Statistical significance was established at $p < 0.05$. * $p < 0.05$, ** $p < 0.01$, *** $p < 0.001$.

## 3. Results and discussion

### 3.1. Synthesis of SS-PI-MA and HA-Cys-Tet

In order to achieve a high iodine content necessary for CT imaging without increasing the injection volume, we designed and prepared reductively degradable polyiodixanol, (SS-PI) by poly-addition of cystamine diisocyanate (CDI) to iodixanol with at a iodixanol/CDI molar ratio of 1/2 (Fig. S1). The $^1$H NMR spectrum of the resulting SS-PI

showed besides resonances due to iodixanol moieties, signals at δ 2.83 and 3.27 attributable to the methylene protons of CDI moieties (Fig. S2). The integral ratio of signals at δ 2.83 (methylene protons of CDI moieties next to the disulfide bond) and 1.76 (methyl protons of iodixanol moieties) revealed that SS-PI had a composition close to the feed molar ratio. GPC data showed that SS-PI had a $M_n$ of 18.8 kg/mol and a $M_w/M_n$ of 1.76. DLS displayed that SS-PI had a size of about 12 nm in DMSO, which was much larger than that of iodixanol (Fig. S3). The treatment of SS-PI with methacrylic anhydride (MA) at a iodixanol/MA molar ratio of 1/1 yielded SS-PI-MA with on the average 0.6 molecules of MA per iodixanol unit in the polymer, as calculated by comparing the integrals of signals at δ 1.89 (methyl protons of MA) to 1.76 (methyl protons of iodixanol moieties) in the $^1$H NMR spectrum (Fig. S4).

HA-Cys-Tet was synthesized by conjugating Tet-Cys-$NH_2$ to the carboxyl groups of HA *via* amidation (Fig. S1). $^1$H NMR clearly showed besides signals attributable to HA also resonances at δ 2.21, 2.71, 7.61-8.22 assignable to Tet-Cys-$NH_2$ moieties (Fig. S5). The degree of substitution (DS) of Tet was determined to be 5 by comparing the integrals of signals at δ 7.61-8.22 (Tet) and δ 1.81 (anomeric proton in HA). UV measurement of Tet moieties at 280 nm confirmed that HA-Cys-Tet had a DS of 5.

### 3.2. Preparation of nanogels and triggered drug release

Hyaluronic acid-iodixanol nanogels (HAI-NGs) were readily obtained *via* nanoprecipitaion and photo-click crosslinking reaction from HA-Cys-Tet and SS-PI-MA. Fig. 1A shows that HAI-NGs had a small size of about 90 nm with a low polydispersity (PDI) of 0.11. TEM confirmed that HAI-NGs had a homogenous size distribution and spherical morphology (Fig. 1B). Notably, HAI-NGs emitted bright green fluorescence under UV light (Fig. 1C inset), which derives from pyrazoline cycloadducts produced by the "tetrazole-alkene" photo-click reaction [36,43]. Fluorescence spectroscopy displayed that HAI-NGs had a strong emission at *ca.* 485 nm (Fig. 1C). The strong fluorescence of HAI-NGs can be used to monitor their *in vitro* and *in vivo* fate. HAI-NGs displayed

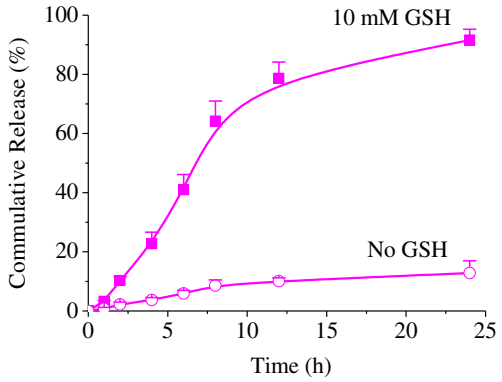


**Fig. 2.** *In vitro* drug release profiles of PTX-loaded HAI-NGs (PTX/HAI-NGs) at pH 7.4 and 37 °C in the presence of 10 mM GSH or without GSH. Data are presented as mean ± SD ($n = 3$).

excellent stability against extensive dilution as well as 10% serum (Fig. S6). However, in the presence of 10 mM glutathione (GSH), HAI-NGs rapidly swelled and agglomerated, supporting their fast redox-responsivity (Fig. 1D).

PTX could be easily loaded into HAI-NGs during nanoprecipitation. A drug loading content (DLC) of 5.9 wt.% was achieved at a theoretical DLC of 10 wt.%. The loading of PTX had little influence on the size and size distribution of HAI-NGs. The *in vitro* release studies showed minimal drug release from PTX-loaded HAI-NGs (*ca.* 10% in 24 h) (Fig. 2). In contrast, nearly complete PTX release was observed in the presence of 10 mM GSH under otherwise the same conditions, probably due to GSH triggered disulfide bond cleavage and de-crosslinking of the nanogels, corroborating that drug release can be accelerated in an intracellular reductive environment. Nanogels typically have a low loading and fast leakage of small molecule drugs [44]. The high PTX loading and inhibited drug leakage of HAI-NGs is likely due to existence of strong π-π interactions between PTX and pyrazoline groups and iodixanol moieties in the nanogels [45].

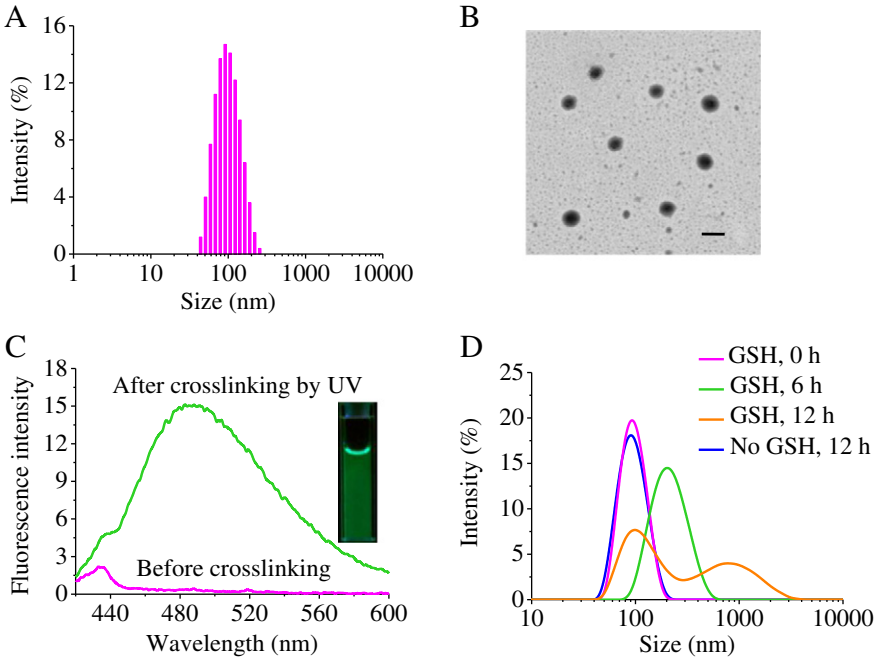


**Fig. 1.** (A) Intensity size distribution of HAI-NGs determined by DLS. (B) TEM image of HAI-NGs (scale bar: 100 nm). (C) Fluorescent spectrum of HAI-NGs before and after crosslinking by UV irradiation. The insert shows a photograph of HAI-NGs under UV light. (D) Triggered destabilization of HAI-NGs in 10 mM GSH.

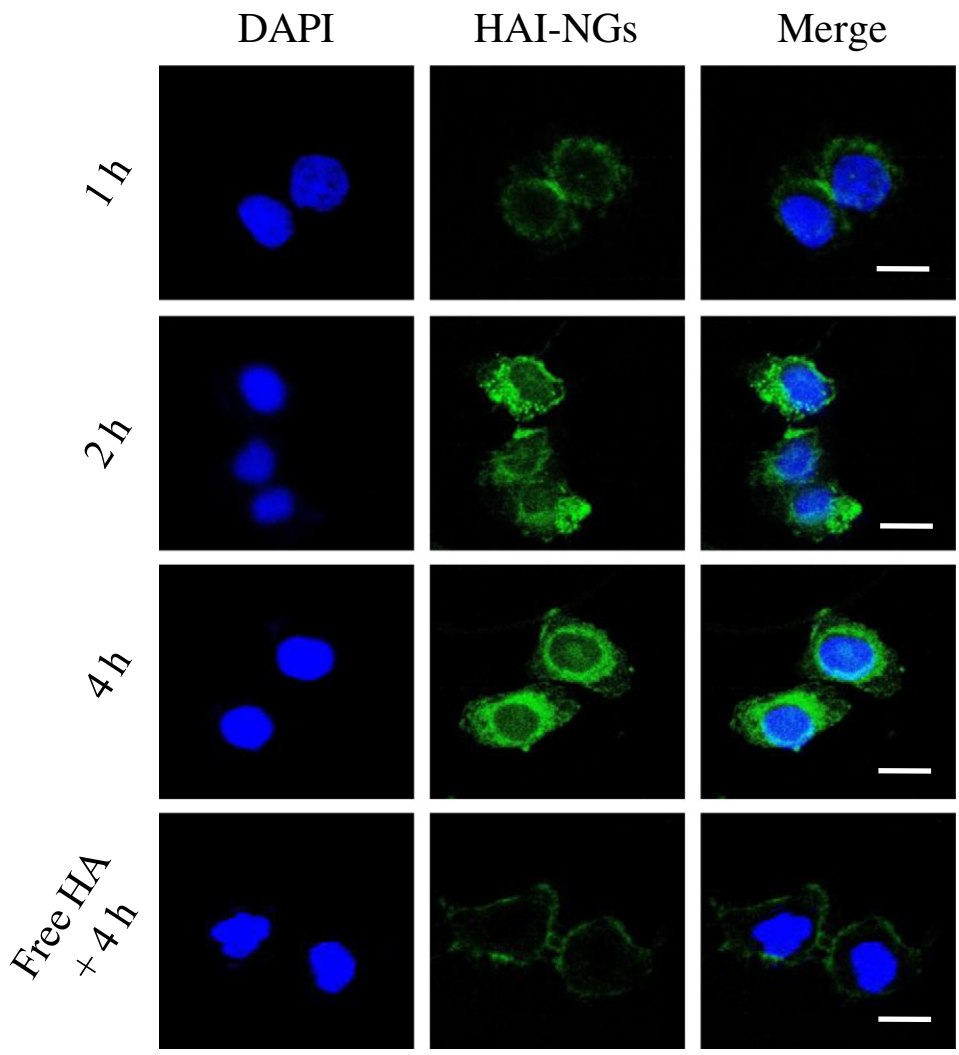


**Fig. 3.** CLSM images of MCF-7 cells following 1 h, 2 h and 4 h incubation with HAI-NGs. Cells pre-treated with free HA (5 mg/mL) for 4 h before adding nanogels were used as a control. The scale bars correspond to 20 μm in all the images.

### 3.3. Cellular uptake and cytotoxicity of PTX-loaded HAI-NGs

Given their strong fluorescence, the cellular uptake of HAI-NGs into CD44 receptor overexpressing MCF-7 breast cancer cells could be conveniently traced by confocal laser scanning microscopy (CLSM). Notably, nanogel fluorescence was clearly observed in MCF-7 cells after 1 h incubation and the fluorescence became stronger at a prolonged incubation time of 2 or 4 h (Fig. 3). The cellular uptake of nanogels was greatly inhibited and only weak nanogel fluorescence was discerned in the cell membrane of MCF-7 cells pre-incubated for 4 h with free HA, demonstrating that

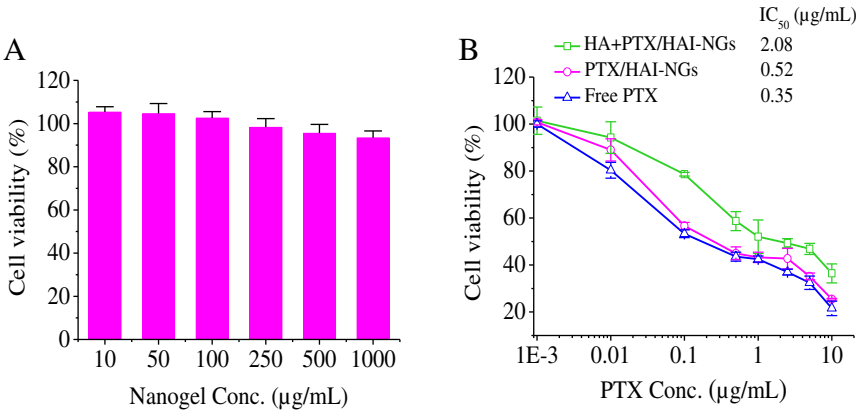


**Fig. 4.** MTT assays of blank HAI-NGs and PTX/HAI-NGs in MCF-7 cells. (A) Viability of MCF-7 cells following 48 h incubation with blank HAI-NGs; and (B) *In vitro* antitumor activity of PTX/HAI-NGs against MCF-7 cells. The cells were incubated with PTX/HAI-NGs for 4 h, the medium was removed and replenished with fresh culture medium, and the cells were cultured for an additional 44 h. The inhibition experiment was performed by pre-treating cells for 4 h with free HA (5 mg/mL) prior to incubation with PTX/HAI-NGs. Data are presented as mean ± SD ($n = 4$).

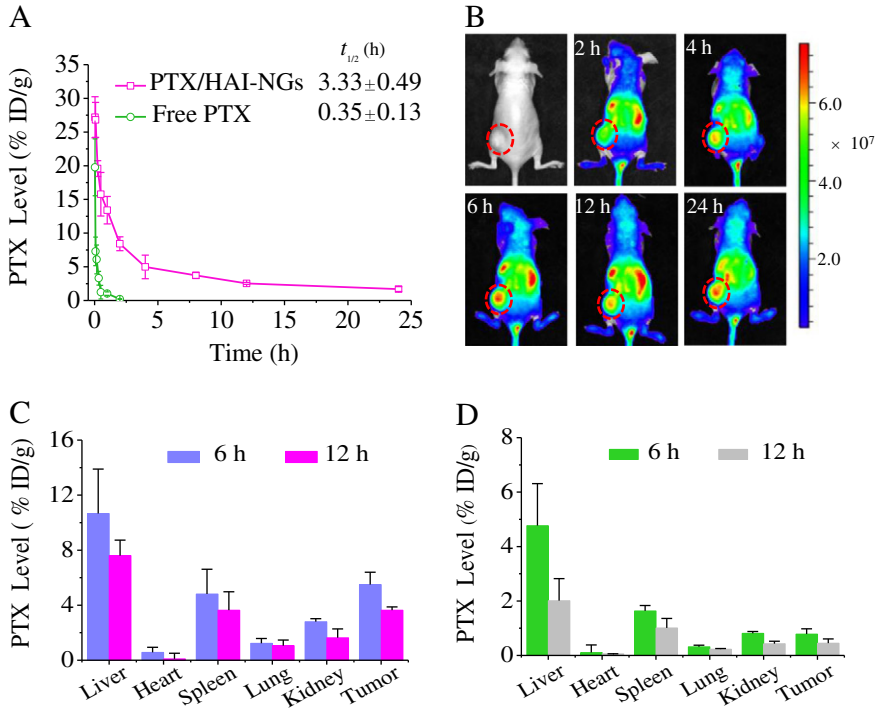


**Fig. 5.** *In vivo* pharmacokinetics, NIR imaging and biodistribution studies. (A) *In vivo* pharmacokinetics of PTX/HAI-NGs and free PTX in mice. PTX level is expressed as % injected dose per gram of tissue (%ID/g). Data are presented as mean ± SD ($n = 3$); (B) *in vivo* fluorescence images of MCF-7 human breast tumor bearing nude mice at different time points following tail vein injection of Cy5-loaded nanogels. Circled areas indicate the locations of the tumor. PTX level, expressed as % injected dose per gram of tissue (%ID/g), in the tumor and different organs after 6 or 12 h post injection of PTX/HAI-NGs (C) or free PTX (D). Data are presented as mean ± SD (n = 3).

HAI-NGs are internalized by MCF-7 cells *via* a receptor-mediated mechanism. Here we also selected L929 murine fibroblastic cells with a low expression of CD44 as negative controls. As shown in Fig. S10, after 4 h incubation, the fluorescence intensity of HAI-NGs in MCF-7 cells was much stronger than that in L929 cells, again proving the cellular uptake of HAI-NGs *via* a CD44-mediated mechanism.

MTT assays showed that blank HAI-NGs were practically non-toxic to MCF-7 cells (>93% cell viability) even at a high nanogel concentration of 1 mg/mL (Fig. 4A), indicating that HAI-NGs possess excellent biocompatibility. In contrast, PTX-loaded HAI-NGs exhibited significant and dose-dependent cytotoxicity against MCF-7 cells (Fig. 4B). The half-maximal inhibitory concentration ($IC_{50}$) of PTX-loaded HAI-NGs was determined to be 0.52 μg/mL, comparable to that of free PTX (0.35 μg/mL), corroborating their efficient cellular internalization and rapid intracellular PTX release. The pre-treatment of MCF-7 cells with free HA for 4 h largely reduced the cytotoxic effect of PTX-loaded HAI-NGs, in line with the above CLSM observations that cellular uptake is inhibited by free HA.

### *3.4. In vivo pharmacokinetics, near infrared imaging and biodistribution of nanogels*

To investigate the *in vivo* pharmacokinetics, PTX-loaded HAI-NGs were *i.v.* injected into BALB/c nude mice at 5 mg PTX/kg and the plasma levels of PTX at different time points were determined by HPLC. Fig. 5A displays that PTX-loaded HAI-NGs had a prolonged circulation time with an elimination half-life of 3.3 h. indicating that nanogels are stable in the circulation and drug leakage is low as a result of strong π-π interactions between PTX and pyrazoline groups

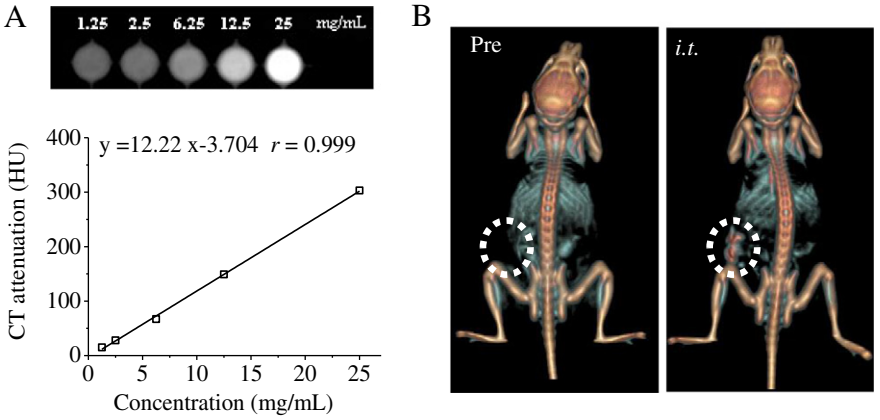


**Fig. 6.** (A) HU measurements of HAI-NGs. The plot showed a linear correlation of CT calculated solution attenuation measured in Hounsfield units (HU) to HAI-NGs at varying concentrations from 1.25 to 25 mg/mL. (B) three-dimensional reconstructed CT images of the MCF-7 tumor bearing mice following intratumoral (*i.t.*) injection of 50 μL of HAI-NGs at a concentration of 15 mg/mL (60 mg iodine equiv./kg). Circled areas indicate the location of the tumor.

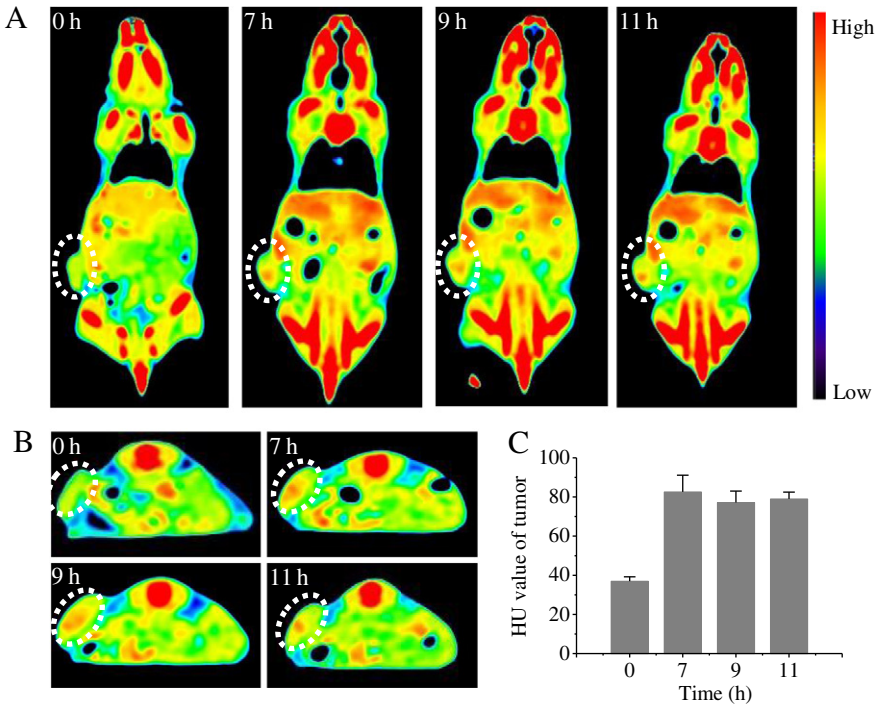


**Fig. 7.** Axial CT images (A), coronal CT images (B) and HU value (C) of MCF-7 tumor bearing mice at 0 h, 7 h, 9 h and 11 h following tail vein injection of HAI-NGs at a concentration of 15 mg/mL (60 mg iodine equiv./kg). Circled areas indicate the position of the tumor.

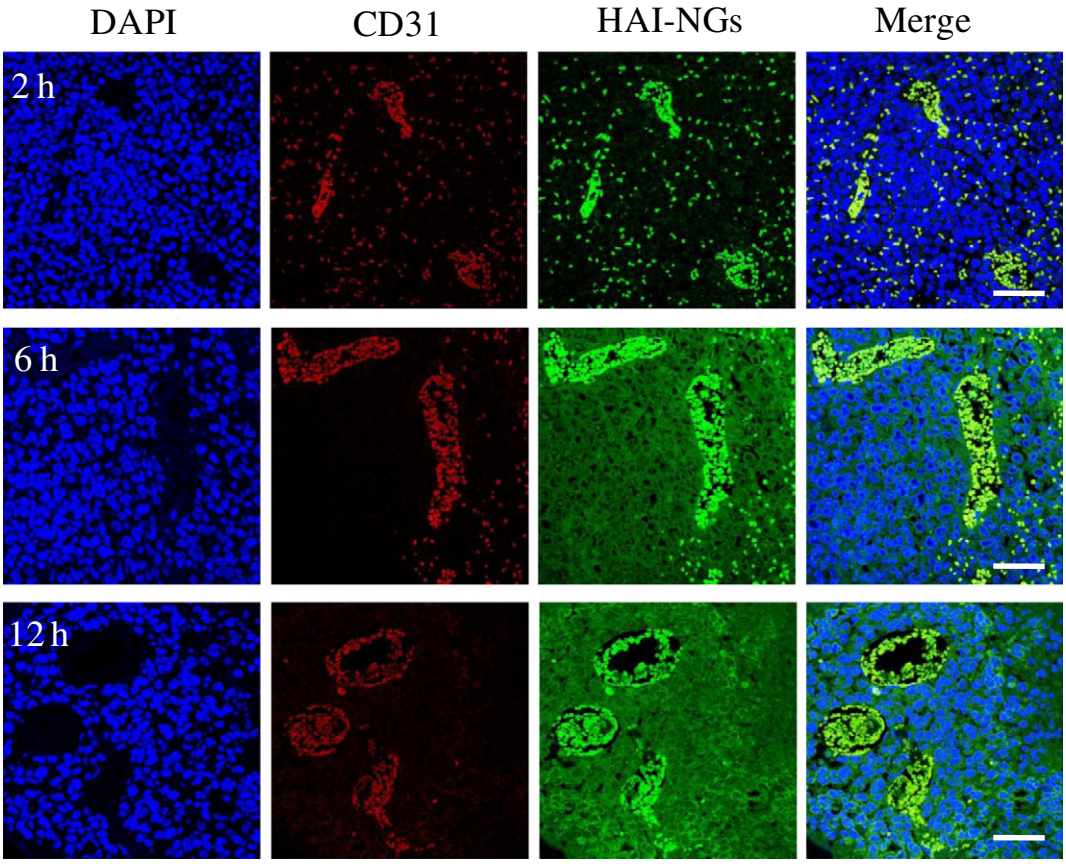


**Fig. 8.** Tumor penetration of HAI-NGs observed by confocal microscopy. Tumor sections were obtained from MCF-7 tumor bearing mice following 2, 6 and 12 h tail vein injection of HAI-NGs (10 mg/mL). The nuclei were stained with DAPI (blue) and blood vessels were stained with CD31 (red). HAI-NGs have an intrinsic green fluorescence. The scale bar represents 50 μm.

and iodixanol moieties in the nanogels [45]. In comparison, free PTX was rapidly eliminated from the blood circulation, with an extremely short half-life time of 0.35 h.

To visualize their tumor accumulation *in vivo*, a near infrared dye Cy5 was loaded into HAI-NGs, and the serum Cy5 release was evaluated. Fig. S11 showed that Cy5 release from HAI-NGs was slow and within 24 h only 4.1% was released. Therefore it is envisaged that Cy5 loaded HAI-NGs are also relatively stable in the circulation. Fig. 5B shows real-time images of Cy5-loaded HAI-NGs in MCF-7 tumor-bearing mice. Notably, tumor accumulation of nanogels was clearly observed at 2 h post injection and reached a maximum at 6 h. This high tumor targeting efficiency of nanogels is likely due to their small size, high stability, and active targeting effect. Interestingly, the fluorescence at the tumor site at 24 h again became stronger compared with that at 12 h, probably because the Cy5 fluorescence is partly self-quenched when loaded into the HAI-NGs due to the homo Förster resonance energy transfer (homo-FRET) effect [46]. When Cy5 molecules are partly released from the disassembled HAI-NGs in the reductive environment, the fluorescence of Cy5 in the tumor area may increase again. It is also noticed that besides in the tumor site, strong fluorescence was also observed in the liver and spleen, probably because after *i.v.* injection, nanogels are also captured by the RES system (mainly liver and spleen). As CD44 receptors are also expressed on liver and spleen cells, uptake of part of the nanogels by these organs may be inevitable".

To profile the *in vivo* biodistribution of PTX-loaded HAI-NGs in MCF-7 tumor bearing mice, PTX levels in the tumor and different organs at 6 and 12 h post injection were quantitatively determined by HPLC. Notably, PTX-loaded nanogels exhibited a high tumor accumulation with 5.5%ID/g at 6 h (Fig. 5C). The tumor PTX accumulation remained high (3.6%ID/g) at 12 h post injection. In comparison, free PTX displayed 7- and 15-fold lower tumor accumulation than PTX-loaded HAI-NGs at 6 and 12 h post injection, respectively (Fig. 5D *versus* Fig. 5C). The PTX level expressed in %ID for the tissues after injection with PTX/HAI-NGs also showed a relatively high retention of PTX in tumor tissue besides the high level in liver tissue and lower levels in the spleen (Fig. S7A). The levels after the administration of free PTX were given in Fig. S7B. The pharmacokinetics, NIR imaging and biodistribution studies all point out that PTX-loaded HAI-NGs have a prolonged circulation time and significantly enhance PTX accumulation in the MCF-7 tumor.

### 3.5. Enhanced CT imaging by HAI-NGs

HAI-NGs can be used for CT imaging due to the presence of a high content of iodixanol. Fig. 6A shows clearly that HAI-NGs effectively enhanced the CT contrast *in vitro*. The corresponding Hounsfield units (HU) values exhibited a linear correlation with HAI-NGs concentrations, suggesting that HAI-NGs can be used for quantitative CT studies. We then evaluated the application of HAI-NGs for *in vivo* CT diagnosis. Interestingly, 5 min after intratumoral (*i.t.*) injection of 50 μL of HAI-NGs at an HAI-NGs concentration of 15 mg/mL (*i.e.* 60 mg iodine equiv./kg) into MCF-7 tumor bearing nude mice, remarkably enhanced contrast was observed at the tumor site in the three-dimensional reconstructed images, with a marked increase of HU value from 37.2 to 182.8 (Fig. 6B). We further investigated whether HAI-NGs can be applied for targeted CT imaging of CD44 overexpressed tumors. The results showed that enhanced contrast was discerned in the MCF-7 tumor from both axial and coronal CT images, with HU values increasing from 37.0 to 82.6, at 7 h following intravenous injection of HAI-NGs into MCF-7 tumor bearing nude mice (Fig. 7). The enhanced tumor contrast further confirms that HAI-NGs can target to and accumulate in the MCF-7 tumor. Notably, the high contrast signal at the tumor site lasted for a long time, which is advantageous for clinical diagnosis. In sharp contrast, little enhancement of HU value was observed at the tumor site for iodixanol (small molecule contrast agent) at the same iodine dose (Fig. S8). Iodixanol was rapidly cleared from the body to the bladder (Fig. S9). It is clear, therefore, that HAI-NGs are superior to iodixanol in targeted CT imaging of CD44 positive tumors.

### 3.6. In vivo tumor penetration and therapeutic efficacy of PTX-loaded HAI-NGs

In the process of tumor-targeted drug delivery, a series of biological barriers may influence the final therapeutic efficacy, among which are interstitial hindrance and tumor penetration [47,48]. The strong intrinsic fluorescence of HAI-NGs was utilized to track their distribution. The blood vessels and cell nuclei were stained by CD31 antibody and DAPI, respectively. Fig. 8 reveals that HAI-NGs were located in the blood vessels at 2 h post *i.v.* injection. At a prolonged time of 6 h post injection, HAI-NGs extravagated from blood vessels to the interstitial space, displaying green fluorescence throughout the whole tumor. At 12 h post injection, HAI-NGs penetrated further deep into the tumor and were actively endocytosed by tumor cells, presenting bright green fluorescence around the cell nuclei. The above phenomena suggest that our HAI-NGs possess good tumor penetration ability.

The antitumor efficacy of PTX-loaded HAI-NGs was evaluated in MCF-7 tumor bearing mice at a dose of 5 mg PTX equiv./kg. The results showed that PTX-loaded HAI-NGs exhibited effective inhibition of tumor growth, which was significantly better than that of free PTX (Fig. 9A). The photographs of tumor blocks excised on day 24 further confirmed that mice treated with PTX-loaded HAI-NGs had the smallest tumor size (Fig. 9B). Both PTX-loaded HAI-NGs and free PTX caused no change of mice body weight (Fig. 9C). Importantly, survival curves showed that PTX-loaded HAI-NGs effectively prolonged the survival time of the MCF-7 breast tumor bearing mice with all mice surviving over an experimental period of 65 d (Fig. 9D). In contrast, mice treated with free PTX and PBS had a median survival time of 40 and 28 d, respectively. The histological analyses by H&E staining displayed that PTX-loaded HAI-NGs induced widespread necrosis of tumor tissue with little damage to the healthy organs including heart, liver and kidney (Fig. 9E), supporting that PTX-loaded HAI-NGs cause low systemic side effects. In comparison, hepatocellular necrosis (red arrows) was observed for free PTX treated mice, similar to previous reports [49,50]. It is evident that PTX-loaded HAI-NGs have low systemic toxicity and mediate efficient and targeted delivery of PTX to human breast tumors *in vivo*, resulting in effective suppression of tumor growth and markedly prolonged survival time.

## 4. Conclusions

We have demonstrated for the first time that bioresponsive and fluorescent hyaluronic acid-iodixanol nanogels (HAI-NGs) mediate targeted X-ray computed tomography (CT) imaging and chemotherapy of MCF-7 human breast tumor *in vivo*. Notably, HAI-NGs have integrated multiple functions including excellent biocompatibility, bright green fluoresence, high stability, superior targetability to CD44 overexpressing cells and fast glutathione-responsive drug release. The *in vivo* studies clearly show that PTX-loaded HAI-NGs have a prolonged circulation time, high tumor accumulation and enhanced tumor penetration in MCF-7 breast tumor-bearing nude mice, resulting in effective tumor growth inhibition, markedly improved survial rate, and reduced systemic toxicity as compared to free PTX. Furthermore, HAI-NGs *via* either intratumoral or intravenous injection leads to significantly enhanced CT imaging of MCF-7 breast tumors in nude mice as compared to iodoxanol. HAI-NGs provide a highly versatile and targeted theranostic nanoplatform that elegantly combines CT imaging with targeted chemotherapy toward CD44 overexpressing tumors.

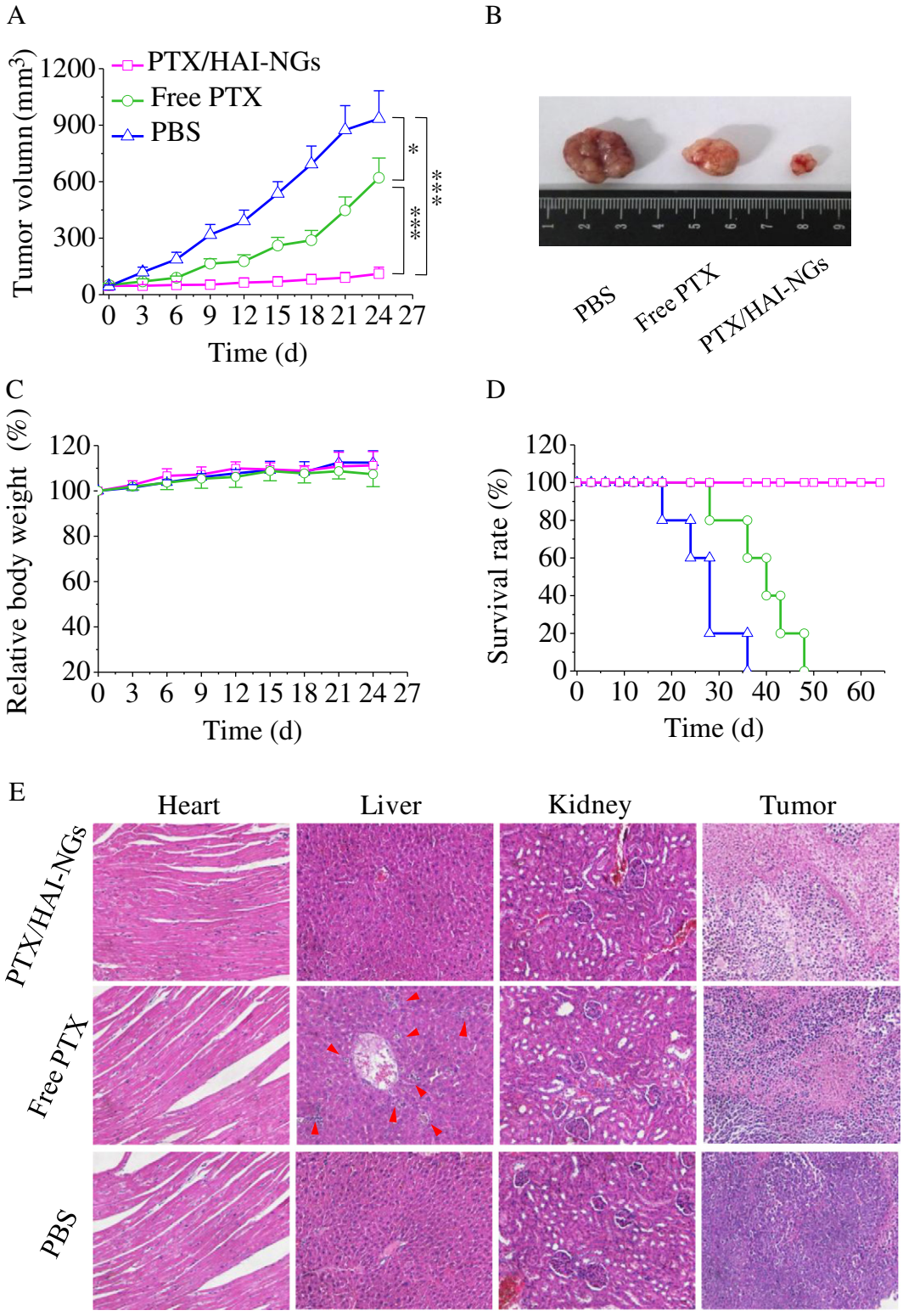


**Fig. 9.** *In vivo* antitumor efficacy of PTX/HAI-NGs in MCF-7 tumor bearing nude mice. Free PTX and PBS were used as controls. The drug was given on day 0, 3, 6, 9, 12 (drug dosage: 5 mg PTX equiv./kg). (A) Tumor volume changes in time. Data are presented as mean ± SD ($n = 6$). (B) Photographs of tumor blocks collected from different treatment groups on day 24. (C) Body weight changes of nude mice following different treatments within 24 days. (D) Survival rates of mice in different treatment groups within 60 d. Data are presented as means ± SD ($n = 5$). * $p < 0.05$, *** $p < 0.001$. (E) H&E stained heart, liver, kidney and tumor sections excised from MCF-7 human breast tumor-bearing mice following 24 d treatment with PTX/HAI-NGs, free PTX or PBS. The images were obtained by a Leica microscope at 200× magnification. Red arrows indicate hepatocellular necrosis.

**Acknowledgements**

This work is financially supported by research grants from the National Natural Science Foundation of China (NSFC 51273139, 51273137 and 51473110), the National Science Fund for Distinguished Young Scholars (NSFC 51225302), and a Project Funded by the Priority Academic Program Development of Jiangsu Higher Education Institutions (PAPD).

## Appendix A. Supplementary data

Supplementary data to this article can be found online at http://dx.doi.org/10.1016/j.jconrel.2016.08.027.

## References


[1] T. Lammers, S. Aime, W.E. Hennink, G. Storm, F. Kiessling, Theranostic nanomedicine, Acc. Chem. Res. 44 (2011) 1029–1038.
[2] X. Ma, Y. Zhao, X.-J. Liang, Theranostic nanoparticles engineered for clinic and pharmaceutics, Acc. Chem. Res. 44 (2011) 1114–1122.
[3] J.H. Ryu, H. Koo, I.-C. Sun, S.H. Yuk, K. Choi, K. Kim, I.C. Kwon, Tumor-targeting multi-functional nanoparticles for theragnosis: new paradigm for cancer therapy, Adv. Drug Deliv. Rev. 64 (2012) 1447–1458.
[4] D.-E. Lee, H. Koo, I.-C. Sun, J.H. Ryu, K. Kim, I.C. Kwon, Multifunctional nanoparticles for multimodal imaging and theragnosis, Chem. Soc. Rev. 41 (2012) 2656–2672.
[5] N. Lee, S.H. Choi, T. Hyeon, Nano-sized CT contrast agents, Adv. Mater. 25 (2013) 2641–2660.
[6] F. Hallouard, N. Anton, P. Choquet, A. Constantinesco, T. Vandamme, Iodinated blood pool contrast media for preclinical X-ray imaging applications–a review, Biomaterials 31 (2010) 6249–6268.
[7] Y. Liu, K. Ai, L. Lu, Nanoparticulate X-ray computed tomography contrast agents: from design validation to in vivo applications, Acc. Chem. Res. 45 (2012) 1817–1827.
[8] H. Lusic, M.W. Grinstaff, X-ray-computed tomography contrast agents, Chem. Rev. 113 (2012) 1641–1666.
[9] E. Jin, Z.-R. Lu, Biodegradable iodinated polydisulfides as contrast agents for CT angiography, Biomaterials 35 (2014) 5822–5829.
[10] K.Y. Choi, G. Liu, S. Lee, X. Chen, Theranostic nanoplatforms for simultaneous cancer imaging and therapy: current approaches and future perspectives, Nanoscale 4 (2012) 330–342.
[11] N. Anton, T.F. Vandamme, Nanotechnology for computed tomography: a real potential recently disclosed, Pharm. Res. 31 (2014) 20–34.
[12] D.P. Cormode, P.C. Naha, Z.A. Fayad, Nanoparticle contrast agents for computed tomography: a focus on micelles, Contrast Media Mol. Imaging 9 (2014) 37–52.
[13] X. Li, N. Anton, G. Zuber, T. Vandamme, Contrast agents for preclinical targeted X-ray imaging, Adv. Drug Deliv. Rev. 76 (2014) 116–133.
[14] J.-Y. Lee, S.-J. Chung, H.-J. Cho, D.-D. Kim, Iodinated hyaluronic acid oligomer-based nanoassemblies for tumor-targeted drug delivery and cancer imaging, Biomaterials 85 (2016) 218–231.
[15] H. Deng, Y. Zhong, M. Du, Q. Liu, Z. Fan, F. Dai, X. Zhang, Theranostic self-assembly structure of gold nanoparticles for NIR photothermal therapy and X-ray computed tomography imaging, Theranostics 4 (2014) 904–918.
[16] J. Zhu, L. Zheng, S. Wen, Y. Tang, M. Shen, G. Zhang, X. Shi, Targeted cancer theranostics using alpha-tocopheryl succinate-conjugated multifunctional dendrimer-entrapped gold nanoparticles, Biomaterials 35 (2014) 7635–7646.
[17] Y. Jiang, J. Chen, C. Deng, E.J. Suuronen, Z. Zhong, Click hydrogels, microgels and nanogels: emerging platforms for drug delivery and tissue engineering, Biomaterials 35 (2014) 4969–4985.
[18] A.V. Kabanov, S.V. Vinogradov, Nanogels as pharmaceutical carriers: finite networks of infinite capabilities, Angew. Chem. Int. Ed. 48 (2009) 5418–5429.
[19] X. Zhang, S. Malhotra, M. Molina, R. Haag, Micro-and nanogels with labile crosslinks-from synthesis to biomedical applications, Chem. Soc. Rev. 44 (2015) 1948–1973.
[20] W. Chen, K. Achazi, B. Schade, R. Haag, Charge-conversional and reduction-sensitive poly (vinyl alcohol) nanogels for enhanced cell uptake and efficient intracellular doxorubicin release, J. Control. Release 205 (2015) 15–24.
[21] N. Morimoto, S. Hirano, H. Takahashi, S. Loethen, D.H. Thompson, K. Akiyoshi, Self-assembled pH-sensitive cholesteryl pullulan nanogel as a protein delivery vehicle, Biomacromolecules 14 (2013) 56–63.
[22] L. Jiang, Q. Zhou, K. Mu, H. Xie, Y. Zhu, W. Zhu, Y. Zhao, H. Xu, X. Yang, pH/temperature sensitive magnetic nanogels conjugated with Cy5.5-labled lactoferrin for MR and fluorescence imaging of glioma in rats, Biomaterials 34 (2013) 7418–7428.
[23] D. Steinhilber, M. Witting, X. Zhang, M. Staegemann, F. Paulus, W. Friess, S. Küchler, R. Haag, Surfactant free preparation of biodegradable dendritic polyglycerol nanogels by inverse nanoprecipitation for encapsulation and release of pharmaceutical biomacromolecules, J. Control. Release 169 (2013) 289–295.
[24] H. Yang, Q. Wang, W. Chen, Y. Zhao, T. Yong, L. Gan, H. Xu, X. Yang, Hydrophilicity/hydrophobicity reversable and redox-sensitive nanogels for anticancer drug delivery, Mol. Pharm. 12 (2015) 1636–1647.
[25] X. Zhang, K. Achazi, D. Steinhilber, F. Kratz, J. Dernedde, R. Haag, A facile approach for dual-responsive prodrug nanogels based on dendritic polyglycerols with minimal leaching, J. Control. Release 174 (2014) 209–216.
[26] C. Yang, X. Wang, X. Yao, Y. Zhang, W. Wu, X. Jiang, Hyaluronic acid nanogels with enzyme-sensitive cross-linking group for drug delivery, J. Control. Release 205 (2015) 206–217.
[27] W. Chen, M. Zheng, F. Meng, R. Cheng, C. Deng, J. Feijen, Z. Zhong, In situ forming reduction-sensitive degradable nanogels for facile loading and triggered intracellular release of proteins, Biomacromolecules 14 (2013) 1214–1222.
[28] X. Wei, T.H. Senanayake, G. Warren, S.V. Vinogradov, Hyaluronic acid-based nanogel-drug conjugates with enhanced anticancer activity designed for the targeting of CD44-positive and drug-resistant tumors, Bioconjug. Chem. 24 (2013) 658–668.
[29] T.F. Stefanello, A. Szarpak-Jankowska, F. Appaix, B. Louage, L. Hamard, B.G. De Geest, B. van der Sanden, C.V. Nakamura, R. Auzély-Velty, Thermoresponsive hyaluronic acid nanogels as hydrophobic drug carrier to macrophages, Acta Biomater. 10 (2014) 4750–4758.
[30] K. Liang, S. Ng, F. Lee, J. Lim, J.E. Chung, S.S. Lee, M. Kurisawa, Targeted intracellular protein delivery based on hyaluronic acid-green tea catechin nanogels, Acta Biomater. 33 (2016) 142–152.
[31] J.J. Water, Y. Kim, M.J. Maltesen, H. Franzyk, C. Foged, H.M. Nielsen, Hyaluronic acid-based nanogels produced by microfluidics-facilitated self-assembly improves the safety profile of the cationic host defense peptide novicidin, Pharm. Res. 32 (2015) 2727–2735.
[32] K. Park, M.-Y. Lee, K.S. Kim, S.K. Hahn, Target specific tumor treatment by VEGF siRNA complexed with reducible polyethyleneimine-hyaluronic acid conjugate, Biomaterials 31 (2010) 5258–5265.
[33] Y. Zhong, J. Zhang, R. Cheng, C. Deng, F. Meng, F. Xie, Z. Zhong, Reversibly crosslinked hyaluronic acid nanoparticles for active targeting and intelligent delivery of doxorubicin to drug resistant CD44+ human breast tumor xenografts, J. Control. Release 205 (2015) 144–154.
[34] E.J. Oh, K. Park, K.S. Kim, J. Kim, J.-A. Yang, J.-H. Kong, M.Y. Lee, A.S. Hoffman, S.K. Hahn, Target specific and long-acting delivery of protein, peptide, and nucleotide therapeutics using hyaluronic acid derivatives, J. Control. Release 141 (2010) 2–12.
[35] J.K. Park, J.H. Shim, K.S. Kang, J. Yeom, H.S. Jung, J.Y. Kim, K.H. Lee, T.H. Kim, S.Y. Kim, D.W. Cho, Solid free-form fabrication of tissue-engineering scaffolds with a poly (lactic-co-glycolic acid) grafted hyaluronic acid conjugate encapsulating an intact bone morphogenetic protein-2/poly (ethylene glycol) complex, Adv. Funct. Mater. 21 (2011) 2906–2912.
[36] Y. Fan, C. Deng, R. Cheng, F. Meng, Z. Zhong, In situ forming hydrogels via catalyst-free and bioorthogonal "tetrazole-alkene" photo-click chemistry, Biomacromolecules 14 (2013) 2814–2821.
[37] W. Song, Y. Wang, J. Qu, Q. Lin, Selective functionalization of a genetically encoded alkene-containing protein via "photoclick chemistry" in bacterial cells, J. Am. Chem. Soc. 130 (2008) 9654–9655.
[38] S. Ganesh, A.K. Iyer, F. Gattacceca, D.V. Morrissey, M.M. Amiji, In vivo biodistribution of siRNA and cisplatin administered using CD44-targeted hyaluronic acid nanoparticles, J. Control. Release 172 (2013) 699–706.
[39] J. Li, M. Huo, J. Wang, J. Zhou, J.M. Mohammad, Y. Zhang, Q. Zhu, A.Y. Waddad, Q. Zhang, Redox-sensitive micelles self-assembled from amphiphilic hyaluronic acid-deoxycholic acid conjugates for targeted intracellular delivery of paclitaxel, Biomaterials 33 (2012) 2310–2320.
[40] H.-j. Yao, Y.-g. Zhang, L. Sun, Y. Liu, The effect of hyaluronic acid functionalized carbon nanotubes loaded with salinomycin on gastric cancer stem cells, Biomaterials 35 (2014) 9208–9223.
[41] P. Kesharwani, S. Banerjee, S. Padhye, F.H. Sarkar, A.K. Iyer, Hyaluronic acid engineered nanomicelles loaded with 3,4-difluorobenzylidene curcumin for targeted killing of CD44+ stem-like pancreatic cancer cells, Biomacromolecules 16 (2015) 3042–3053.
[42] X. Wang, J. Zhang, R. Cheng, F. Meng, C. Deng, Z. Zhong, Facile synthesis of reductively degradable biopolymers using cystamine diisocyanate as a coupling agent, Biomacromolecules 17 (2016) 882–890.
[43] Z. Yu, L.Y. Ho, Q. Lin, Rapid, photoactivatable turn-on fluorescent probes based on an intramolecular photoclick reaction, J. Am. Chem. Soc. 133 (2011) 11912–11915.
[44] J. Peng, T. Qi, J. Liao, M. Fan, F. Luo, H. Li, Z. Qian, Synthesis and characterization of novel dual-responsive nanogels and their application as drug delivery systems, Nanoscale 4 (2012) 2694–2704.
[45] Y. Shi, M.J. van Steenbergen, E.A. Teunissen, L.S. Novo, S. Gradmann, M. Baldus, C.F. van Nostrum, W.E. Hennink, π–π stacking increases the stability and loading capacity of thermosensitive polymeric micelles for chemotherapeutic drugs, Biomacromolecules 14 (2013) (1826-1837).
[46] H. Kobayashi, P.L. Choyke, Target-cancer-cell-specific activatable fluorescence imaging probes: rational design and in vivo applications, Acc. Chem. Res. 44 (2010) 83–90.
[47] V.P. Chauhan, R.K. Jain, Strategies for advancing cancer nanomedicine, Nat. Mater. 12 (2013) 958–962.
[48] R.K. Jain, T. Stylianopoulos, Delivering nanomedicine to solid tumors, Nat. Rev. Clin. Oncol. 7 (2010) 653–664.
[49] L. Liang, S.-W. Lin, W. Dai, J.-K. Lu, T.-Y. Yang, Y. Xiang, Y. Zhang, R.-T. Li, Q. Zhang, Novel cathepsin B-sensitive paclitaxel conjugate: higher water solubility, better efficacy and lower toxicity, J. Control. Release 160 (2012) 618–629.
[50] Y. Zou, Y. Song, W. Yang, F. Meng, H. Liu, Z. Zhong, Galactose-installed photo-crosslinked pH-sensitive degradable micelles for active targeting chemotherapy of hepatocellular carcinoma in mice, J. Control. Release 193 (2014) 154–161.